LETTER

doi:10.1038/nature14586

DNA rendering of polyhedral meshes at the nanoscale

Erik Benson[1,2], Abdulmelik Mohammed[3], Johan Gardell[1,2], Sergej Masich[4], Eugen Czeizler[3], Pekka Orponen[3] & Björn Högberg[1,2]

It was suggested[1] more than thirty years ago that Watson–Crick base pairing might be used for the rational design of nanometre-scale structures from nucleic acids. Since then, and especially since the introduction of the origami technique[2], DNA nanotechnology has enabled increasingly more complex structures[3–18]. But although general approaches for creating DNA origami polygonal meshes and design software are available[14,16,17,19–21], there are still important constraints arising from DNA geometry and sense/antisense pairing, necessitating some manual adjustment during the design process. Here we present a general method of folding arbitrary polygonal digital meshes in DNA that readily produces structures that would be very difficult to realize using previous approaches. The design process is highly automated, using a routeing algorithm based on graph theory and a relaxation simulation that traces scaffold strands through the target structures. Moreover, unlike conventional origami designs built from close-packed helices, our structures have a more open conformation with one helix per edge and are therefore stable under the ionic conditions usually used in biological assays.

The starting point of the method we present here is a 3D mesh representing the geometry one wishes to realize at the nanoscale. Focusing only on polyhedral meshes, that is, meshes which enclose a volume inflatable to a ball, and in contrast to several previous approaches[14,17,19] (see Extended Data Fig. 1), we aim to replace the edges of the mesh by single DNA double helices such that the scaffold strand traverses each of these edges once. This problem is closely related to the 'Chinese postman tour' problem[22] in graph theory, and finding solutions by hand would be impossible in practice for most meshes. The main three principles underpinning our design paradigm are: first, that the technique should allow meshes to be triangulated to optimize structural rigidity; second, that each edge should be represented by one double helix to enable construction of large structures using as little DNA as possible (though some meshes require two helices to render certain edges, as discussed below); and, third, that vertices should be non-crossing (that is, the scaffold should not cross itself at the vertices, which ensures non-knotted paths with fewer topological and kinetic traps during folding, and vertex junctions should be planar, which avoids mesh protrusions caused by the stacking of crossing helices at each vertex).

The overall design scheme is split into four discrete steps, as follows. (1) Drawing of a 3D polygon mesh using 3D software; see Fig. 1a. (2) Generating an appropriate routeing of the long scaffold strand through

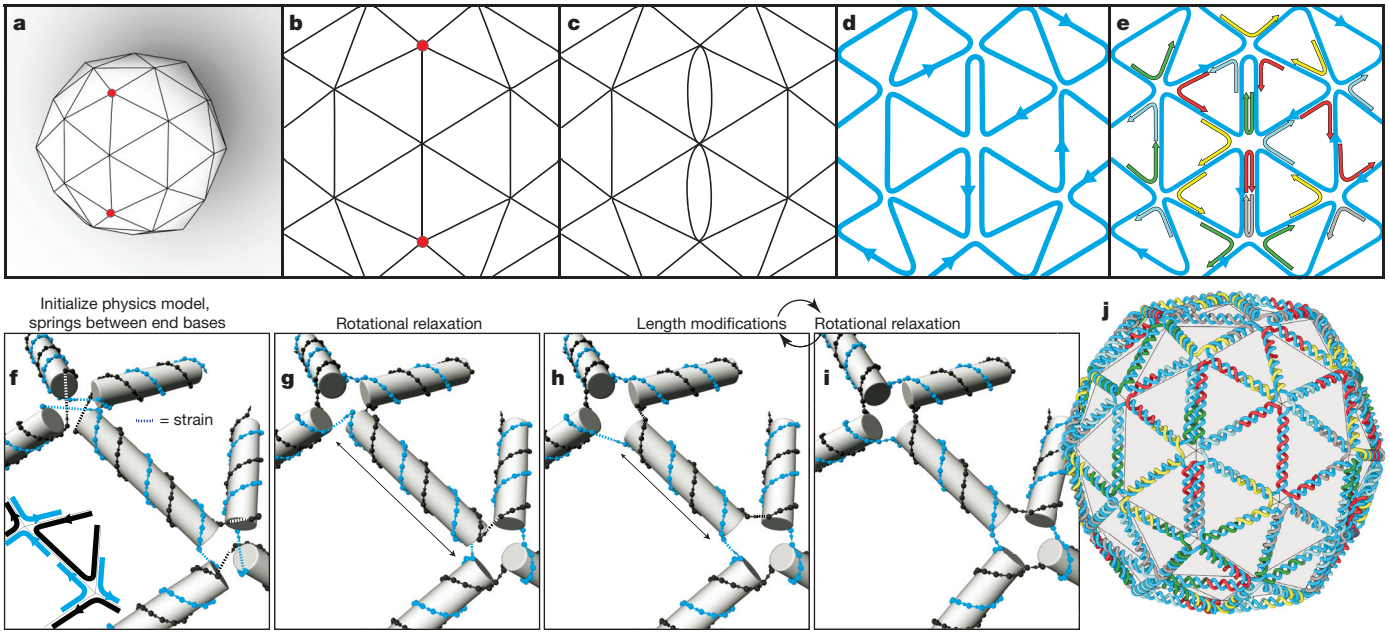

Figure 1 | Design paradigm and automated workflow for scaffold-routeing sequence design of origami 3D meshes. **a**, A 3D mesh is drawn using 3D software. **b**, Using the minimum weight perfect matching algorithm, odd-degree vertices are paired. **c**, Double edges are introduced. **d**, The developed A-trails algorithm routes the scaffold according to the constraints. **e**, The staple-strand (multi-coloured) routeing follows implicitly from the scaffold (blue) routeing. **f–i**, Before computation of the sequences, a physics model is used to relax and evenly distribute strain in the design. Each double helix is treated as a stiff rod with springs connecting the bases at the ends of the scaffold strand and staple strand. Iterations of rotational relaxation (**g** and **i**) and length modification of helices (**h**) leads to the final design (**j**), where sequences are calculated after importing to vHelix.

[1]Department of Medical Biochemistry and Biophysics, Karolinska Institutet, SE-171 77 Stockholm, Sweden. [2]Department of Neuroscience, Karolinska Institutet, SE-171 77 Stockholm, Sweden. [3]Department of Computer Science, Aalto University, FI-00076 Aalto, Finland. [4]Department of Cell and Molecular Biology, Karolinska Institutet, SE-171 77 Stockholm, Sweden.

all the edges of the mesh; see Fig. 1b–e. (3) Determining the least-strained DNA helix arrangement that will realize the desired 3D mesh; see Fig. 1f–i. (4) Optional fine tuning of the design and generation of the staple strands; see Fig. 1j.

Having selected a target 3D polygon mesh (design step (1)), the first condition for a triangulated mesh to be routable (design step (2)), with the scaffold strand traversing every edge once, is that the mesh graph must admit an Eulerian circuit, that is, all its vertices have an even degree. To make meshes Eulerian, we use a general re-conditioning algorithm that adds 'helper edges' by introducing extra helices along certain edges; see Fig. 1b–d. A re-conditioning with the minimum number of additional helper edges, with at most one additional helper helix per edge, amounts to finding a 'minimum weight perfect matching' of odd-degree vertices (compare with Supplementary Fig. 1.1 in Supplementary Note 1). However, Eulerian circuits are not sufficient to ensure scaffold routeing, because such circuits may generally have multiple crossings at many vertices, and even 'elementary non-crossing' circuits cannot always be connected by complementary staple strands (see Supplementary Fig. 1.3 in Supplementary Note 1).

These considerations lead us to adopt a routeing based on A-trails[23], a specific type of Eulerian circuits, where consecutive edges of the circuit are always neighbours in the cyclic ordering around the vertices (exemplified in Fig. 1d). Although there are efficient algorithms for finding Eulerian circuits and for minimum weight perfect matchings[22], it is strongly believed that there is no efficient algorithm for finding A-trails in general graphs, or even in polyhedral graphs[23]; that is, the problem is known to be NP-complete. Nevertheless, by the systematic search we developed, employing pruning and a heuristic for branching, our algorithm managed to find a routeing for all the designed meshes within seconds. (For more detailed discussion of the graph theory guiding our scaffold routeing procedure and the associated algorithm, see Methods and Supplementary Note 1.)

The routeing of the staple strands (the helper DNA oligonucleotides that drive DNA-origami folding) follows implicitly from completing the edge connections at the vertices (Fig. 1e). For design step (3), a physical model of rigid cylinders joined by stressed springs at the vertex junctions is implemented *in silico* and allowed to relax in a simulation to give fewer overlaps and smaller gaps at the vertices. In the case of helices where the routeing complicates the rotational relaxation (that is, where connections on the opposite end of the helix try to rotate the helix in the opposite direction; see Fig. 1g), we add an iterative length-modification step in the relaxation algorithm (Fig. 1h) to adjust the lengths of individual edges. (See Methods and Supplementary Note 2 for a full description of the

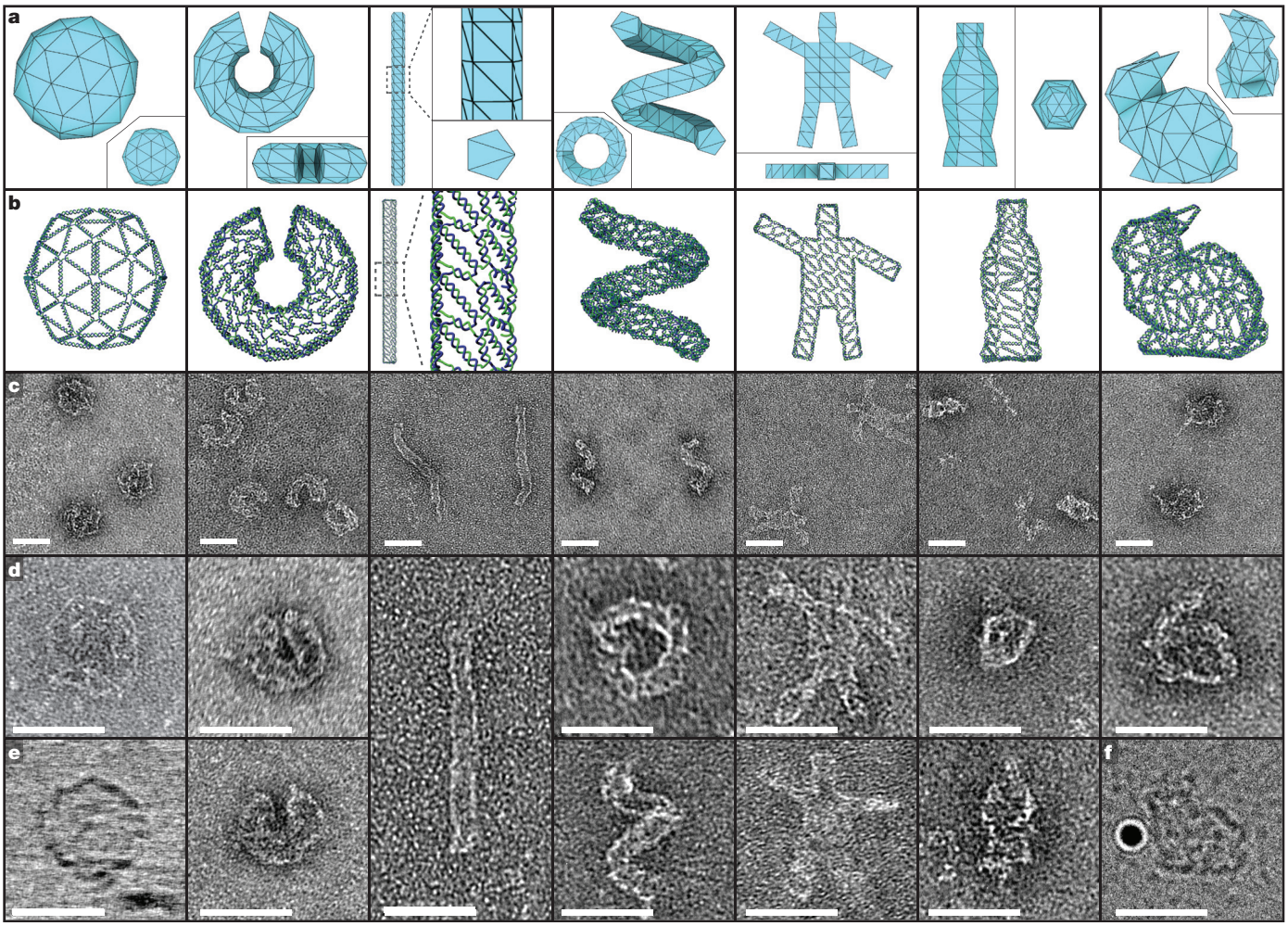

Figure 2 | 3D meshes rendered in DNA. **a**, Different views of the 3D meshes provided as starting points for the automated design process. In columns from left to right: a ball generated by subdivision of an icosahedron, a nicked torus, a rod and a helix with pentagonal cross-sections, a thin, semi-two-dimensional, waving stickman, a bottle and a version of the Stanford bunny. **b**, The front face of the complete DNA designs in each case with single DNA strands rendered as tubes: the staple strands in blue and the scaffold strands in green. **c**–**e**, Negative-stain dry-state transmission electron microscopy (except for the ball and bunny in **e** and **f**, respectively) micrographs of each of the structures. **c**, 250 nm × 250 nm views. **d** and **e** show 100 nm × 100 nm close-ups (excluding the pentagonal rod, which is 200 nm × 100 nm). **e**, **f**, The ball and bunny are imaged using cryo-electron microscopy (the gold particle used for alignment is visible in **f**). Scale bars are 50 nm.

physical relaxation simulation and length-correction process.) The relaxed model is then imported into Autodesk Maya running vHelix (http://www.vhelix.net), a custom-made dedicated plugin for the design and visualization of DNA nanostructures, as shown in Extended Data Fig. 2.

For fine-tuning of the design (optional step (4)), the smaller gaps within the imported relaxed model can be filled with unpaired nucleotides, which will provide flexibility and correct strand misalignments during assembly. If desired, further manual post-processing of the design, such as modifying staple-strand breakpoints, can be done in vHelix. Finally, we introduce the desired scaffold-strand sequence, and then vHelix automatically generates the staple-strand sequences, thus completing the design process.

Overall, the set of tools provided allows a target 3D geometry to be rendered with DNA automatically, with fine-grained control over the design in a graphical user interface before sequence generation. An outline view of the complete pipeline is given in Extended Data Fig. 3.

We designed six polyhedral models in Autodesk Maya: a ball, a nicked torus, a helix, a rod, a humanoid stickman and a soda bottle. From a downloaded and imported model (http://visual.k.u-tokyo.ac.jp/research/unfolding/index-e.html), we also produced a reduced polygon version of the Stanford bunny. We scaled the structures to scaffold sizes of between six and eight thousand nucleotides. The scaling (physical dimension) of each model can be set arbitrarily before the relaxation simulation and will determine the double-helix characteristics at each edge. Implicitly, the scaling also affects the number of edges, or 'resolution', of a polyhedral model that can be rendered from a given strand of DNA of a certain length. That is, the number of edges, combined with the overall size of the object, determines how long the DNA scaffold must be.

The routeing of the staple strands is fully determined by the scaffold routeing. However, the placement of staple-strand breakpoints can be freely modified. In the case of the symmetrical ball structure, we designed the breakpoints using a simple scheme in which each staple strand attaches to two adjacent half-edges of the routed scaffold. In the other structures, which have a larger spread of edge lengths, we implemented an automatic scheme for staple-strand breakpoint design in which staple strands were designed to hybridize (pair) with more than two edges. This avoided breakpoints on the shortest edges, which allowed them to be scaled to a smaller size.

We found in the vHelix models that in some of our target structures, which are complex and strongly curved 3D objects, some of the strands in certain vertices appeared to leave gaps in the junctions and could lead to strain in the final assembly. We therefore implemented a feature in vHelix that relaxes such strands through the addition of extra unpaired bases on either the scaffold strands or on the staple strands in the vertices. When the unpaired bases were placed on the staple strands, we designed them to be adenines. This was implemented for all structures except the ball.

All structures were folded at an excess of 10× staple strands to scaffold strands and evaluated in agarose gel electrophoresis (Supplementary Figs 1–7). Subsequent imaging of the DNA structures in negative-stained transmission electron microscopy (Fig. 2c and d; Supplementary Figs 8–14) revealed objects in good accordance with prediction, although the hollow structures sometimes appear collapsed in the dried-out state of negative-stained transmission electron microscopy. Cryo-electron tomography however, allows imaging of the structures in a hydrated state (Fig. 2e, f, Fig. 3 and Supplementary Figs 15 and 16) and revealed that they did indeed fold into their desired shapes; the tomography even uncovered, in close up, features of the underlying DNA mesh (Fig. 3).

Most DNA origami structures are built from tightly packed helices stabilized by multivalent cations or high concentrations of monovalent cations[24], preventing them from folding and remaining stable in physiological buffer systems. Our new polyhedral structures do not share the close packing of helices, and we found that the ball, helix, nicked torus and stickman folded and remained stable in two buffers commonly used in biomedical research—phosphate buffered saline (PBS) and Dulbecco's Modified Eagle Medium (DMEM)—and when using a classic magnesium-rich buffer (Fig. 4 and Supplementary Figs 17–25). We see some evidence of aggregation when folding in DMEM, which might be alleviated by folding in PBS followed by buffer exchange into DMEM. Compared to standard origami[25], the structures appear more stable in cell culture buffers supplemented with non-inactivated serum (fetal bovine serum) but exhibit similar sensitivity to high concentrations of nuclease (Supplementary Figs 25 and 26; see also Methods).

The ease of the design process is an important parameter for determining whether a new nanotechnology method will find wide use. Because our method is highly amenable to full automation, it opens up the possibility of 'one-click' 3D printing at the nanoscale: the user would draw a polygonal shape in 3D software and would then be directly provided with the DNA sequences to order. The ball, bottle and bunny designs were all generated in such a completely automated fashion, giving DNA structures directly from digital 3D meshes without manual intervention. The paradigm renders structures that fold well with a yield of 5%–92% estimated from agarose gel electrophoresis (Supplementary Figs 1–7, Supplementary Table 1) and where almost all particles examined (from the leading agarose gel band) in cryo-electron tomography appear well formed (Figs 2 and 3; Supplementary Figs 15 and 16).

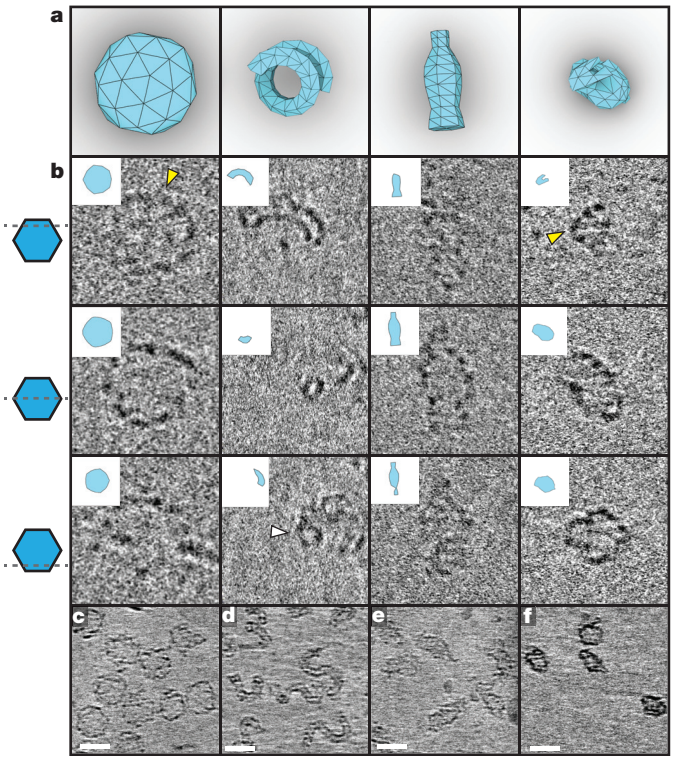

Figure 3 | Cryo-electron microscopy reveals the hollow characteristics and details of polyhedral meshes. From left to right, the ball, helix, bottle and bunny are shown. **a**, 3D renderings of the structures shown in the cryo-electron tomography images in **b** rotated to correspond to the particles observed in the data. **b**, Three progressive slices of the structures reconstructed from cryo-electron tomography imaging. Images are 100 nm × 100 nm wide. Insets show the expected outlines from the corresponding sections of the digital models. Mesh triangulation can be observed (yellow arrows), as well as the pentagonal cross-section of the helix tube (white arrow). **c**–**f**, Overview images from cryo-electron microscopy of each of the structures (contrast projection reconstructions, obtained by averaging multiple tomography slices). Scale bars are 50 nm.

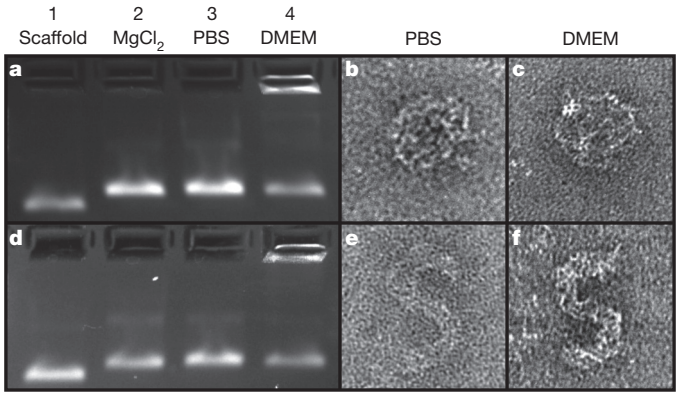

Figure 4 | Mesh origami folds in and is fully stable in physiological buffers. **a**, **d**, Agarose gel electrophoresis of the ball (**a**) and the helix (**d**) folded in different buffers. Scaffold DNA is shown in lane 1. Structures are folded in cell media as follows: in 10 mM $MgCl_2$ and 5 mM Tris (lane 2), in PBS (lane 3) and in DMEM (lane 4). **b**, **c**, **e**, **f**, Transmission electron micrographs of the ball (**b** and **c**), and the helix (**e** and **f**) folded in PBS (**b** and **e**) or DMEM (**c** and **f**). Images are 100 nm × 100 nm wide.

This work is the first to base DNA origami architecture on A-trails routeing theory. But the rational design of small-protein nanostructures using other types of Eulerian paths has also been recently reported[26], further highlighting the value of a deeper mathematical understanding of path routeing in the self-assembly of linear molecules. In this case, by exactly formulating the non-crossing scaffold routeing problem as a search for a specific type of Eulerian circuits in polyhedral graphs and then connecting this search problem to a long-standing conjecture in graph theory concerning the existence of A-trails in planar Eulerian triangulations, we arrived at an effective branch-and-bound search algorithm that makes it feasible to find the requisite scaffold routeings quickly, even in 3D designs with a large polygon count, despite the problem being NP-complete.

We hypothesize that the open folding architecture we present could be particularly well suited for folding using very long staple strands[27] for increased thermal stability in the future. A similar long-staple-strand strategy is believed to be difficult to implement using normal origami routeing owing to the intrinsically high degree of topological complexity.

3D DNA origami has traditionally been implemented using close-packed helices that can yield solid brick-like shapes[14,15] that are both impressive and visually appealing when imaged using dry-state negative-stain transmission electron microscopy. But emerging work[28–30] that utilizes DNA origami in biological research, where qualities such as stability in low-salt conditions and structural flexibility are important, has favoured one-layer, hollow structures. The new design paradigm we report here, using double helices alone as structural elements instead of close-packed bundles of helices, alleviates the need for non-physiological concentrations of salts completely, and is expected to enable more experiments in cell biology and potentially also *in vivo*, with a closer match between conditions in the model system and the true biological context.

Online Content Methods, along with any additional Extended Data display items and Source Data, are available in the online version of the paper; references unique to these sections appear only in the online paper.

Received 24 February; accepted 14 May 2015.

1. Seeman, N. C. Nucleic-acid junctions and lattices. *J. Theor. Biol.* **99,** 237–247 (1982).
2. Rothemund, P. W. K. Folding DNA to create nanoscale shapes and patterns. *Nature* **440,** 297–302 (2006).
3. Chen, J. H. & Seeman, N. C. Synthesis from DNA of a molecule with the connectivity of a cube. *Nature* **350,** 631–633 (1991).
4. Rothemund, P. W. K., Papadakis, N. & Winfree, E. Algorithmic self-assembly of DNA Sierpinski triangles. *PLoS Biol.* **2,** e424 (2004).
5. He, Y., Tian, Y., Ribbe, A. E. & Mao, C. Highly connected two-dimensional crystals of DNA six-point-stars. *J. Am. Chem. Soc.* **128,** 15978–15979 (2006).
6. Shih, W. M., Quispe, J. D. & Joyce, G. F. A 1.7-kilobase single-stranded DNA that folds into a nanoscale octahedron. *Nature* **427,** 618–621 (2004).
7. Goodman, R. P. *et al.* Rapid chiral assembly of rigid DNA building blocks for molecular nanofabrication. *Science* **310,** 1661–1665 (2005).
8. Bhatia, D. *et al.* Icosahedral DNA nanocapsules by modular assembly. *Angew. Chem. Int. Edn Engl.* **48,** 4134–4137 (2009).
9. Geary, C., Rothemund, P. W. K. & Andersen, E. S. A single-stranded architecture for cotranscriptional folding of RNA nanostructures. *Science* **345,** 799–804 (2014).
10. List, J., Weber, M. & Simmel, F. C. Hydrophobic actuation of a DNA origami bilayer structure. *Angew. Chem. Int. Edn Engl.* **53,** 4236–4239 (2014).
11. Andersen, E. S. *et al.* Self-assembly of a nanoscale DNA box with a controllable lid. *Nature* **459,** 73–76 (2009).
12. Marchi, A. N., Saaem, I., Vogen, B. N., Brown, S. & LaBean, T. H. Toward larger DNA origami. *Nano Lett.* **14,** 5740–5747 (2014).
13. Ke, Y. *et al.* Scaffolded DNA origami of a DNA tetrahedron molecular container. *Nano Lett.* **9,** 2445–2447 (2009).
14. Douglas, S. M. *et al.* Self-assembly of DNA into nanoscale three-dimensional shapes. *Nature* **459,** 414–418 (2009).
15. Dietz, H., Douglas, S. & Shih, W. M. Folding DNA into twisted and curved nanoscale shapes. *Science* **325,** 725 (2009).
16. Han, D. *et al.* DNA gridiron nanostructures based on four-arm junctions. *Science* **339,** 1412–1415 (2013).
17. Iinuma, R. *et al.* Polyhedra self-assembled from DNA tripods and characterized with 3D DNA-PAINT. *Science* **344,** 65–69 (2014).
18. Liedl, T., Högberg, B., Tytell, J., Ingber, D. E. & Shih, W. M. Self-assembly of three-dimensional prestressed tensegrity structures from DNA. *Nature Nanotechnol.* **5,** 520–524 (2010).
19. Rothemund, P. W. K. in *Nanotechnology: Science and Computation* (eds Chen, J., Jonoska, N. & Rozenberg, G.) 3–21 (Springer, 2006).
20. Ellis-Monaghan, J. A., McDowell, A., Moffatt, I. & Pangborn, G. DNA origami and the complexity of Eulerian circuits with turning costs. *Natural Comput.*. http://dx.doi.org/10.1007/s11047-014-9457-2 (2014).
21. Douglas, S. M. *et al.* Rapid prototyping of 3D DNA-origami shapes with caDNAno. *Nucleic Acids Res.* **37,** 5001–5006 (2009).
22. Edmonds, J. & Johnson, E. L. Matching, Euler tours and the Chinese postman. *Math. Program.* **5,** 88–124 (1973).
23. Døvling Andersen, L. & Fleischner, H. The NP-completeness of finding A-trails in Eulerian graphs and of finding spanning trees in hypergraphs. *Discrete Appl. Math.* **59,** 203–214 (1995).
24. Martin, T. G. & Dietz, H. Magnesium-free self-assembly of multi-layer DNA objects. *Nature Commun.* **3,** 1103 (2012).
25. Hahn, J., Wickham, S. F. J., Shih, W. M. & Perrault, S. D. Addressing the instability of DNA nanostructures in tissue culture. *ACS Nano* **8,** 8765–8775 (2014).
26. Gradišar, H. *et al.* Design of a single-chain polypeptide tetrahedron assembled from coiled-coil segments. *Nature Chem. Biol.* **9,** 362–366 (2013).
27. Ducani, C., Kaul, C., Moche, M., Shih, W. M. & Högberg, B. Enzymatic production of 'monoclonal stoichiometric' single-stranded DNA oligonucleotides. *Nature Methods* **10,** 647–652 (2013).
28. Shaw, A. *et al.* Spatial control of membrane receptor function using ligand nanocalipers. *Nature Methods* **11,** 841–846 (2014).
29. Douglas, S. M., Bachelet, I. & Church, G. M. A logic-gated nanorobot for targeted transport of molecular payloads. *Science* **335,** 831–834 (2012).
30. Amir, Y. *et al.* Universal computing by DNA origami robots in a living animal. *Nature Nanotechnol.* **9,** 353–357 (2014).

Supplementary Information is available in the online version of the paper.

Acknowledgements This work was funded through grants from the Swedish Research Council (grants 2010-5060 and 2013-5883 to B.H.), the Swedish Foundation for Strategic Research (grant FFL12-0219 to B.H.) and the Knut and Alice Wallenberg foundation (Academy Fellow grant KAW2014.0241 to B.H.). E.B. was also funded by a Wallenberg Scholars grant to O. Inganäs. The work of A.M. was supported by the Helsinki Doctoral Education Network on Information and Communications Technology. We acknowledge the computational resources provided by the Aalto Science-IT project and the use of the Facility for EM Tomography at the Karolinska Institutet. A.M., E.C. and P.O. thank G. García Pérez for help in implementing early variants of the scaffold routing software. We thank P. Kumar Areddy (Karolinska Institutet) and A.-L. Bank Kodal and K. Gothelf (Aarhus University) for help with early experimental testing.

Author Contributions B.H. conceived and designed the study. P.O., E.C. and A.M. performed the theoretical work. E.B. performed the experimental work. A.M. performed most of the algorithm implementation. J.G. collaborated on the algorithm implementation and implemented the relaxation method and the vHelix plug-in. S.M. performed the cryo-electron tomography and tomography with help from E.B. All authors contributed to the writing of the manuscript.

Author Information Reprints and permissions information is available at www.nature.com/reprints. The authors declare no competing financial interests. Readers are welcome to comment on the online version of the paper. Correspondence and requests for materials should be addressed to B.H. (bjorn.hogberg@ki.se).

METHODS

Code availability. Links to source code for all software, instructional videos and tutorials that pertain to the polygonal design process reported can be found at http://www.vhelix.net.

Mesh design. The 3D objects were designed in Autodesk Maya 2014 as polygon objects. The feature "triangulate" was used to triangulate the meshes. Note that fully triangulated convex polyhedral meshes are structurally rigid[31]. When designing meshes, the number of edges was kept to an appropriate amount for the intended scaffold in the downstream design and the spread in edge lengths was kept small.

The routeing algorithm works on meshes in ASCII PLY format. Autodesk Maya does not currently support export in this format, so meshes were exported in the STL format and converted to PLY using the tool meshconv (http://www.cs.princeton.edu/~min/meshconv/).

Routeing and relaxation. The algorithms for reconditioning and routeing of the mesh as well as physically relaxing it for import to vHelix are all performed by running a single BAT file on the mesh file using the command prompt:

bscor.bat model_ply_file *scale*

The decimal value *scale* is used in the physical relaxation where the edges of the mesh are converted into DNA helices of a certain length. The batch script generates a scaffold routeing of the mesh given in PLY file format by executing a sequence of modules. Note that the precise formulation of the scaffold routeing problem and a detailed discussion of the graph-theoretic concepts applied in the modules are available in Supplementary Note 1.

The first module converts the PLY file format into the DIMACS format, which is a widely used representation for graphs. Note that the 3D positioning of the vertices is lost in this conversion. Nevertheless, the relative—that is, cyclic (for example, counter-clockwise)—order of edges around vertices, which is essential information when finding an A-trail routeing, can still be obtained by a planar embedding algorithm in the third step.

The second module applies the reconditioning of the graph if the graph is not Eulerian. The scaffold is able to traverse each edge exactly once if and only if the graph is Eulerian. Hence, once-per-edge scaffold routeing is only possible if there are no odd-degree vertices[32]. Thus, the module identifies the odd-degree vertices and (if such vertices exist) applies Edmonds' blossom algorithm[22] for minimum weight perfect matching. The result of the matching yields a transformation of the initial graph into an Eulerian one by adding a minimum amount of double edges between pairs of odd-degree vertices. If on the other hand there are no odd-degree vertices, the script continues with the original graph.

The third module applies the Boyer–Myrvold algorithm[33] and generates a planar embedding of the graph. Since the input graph is from a polyhedral mesh, it is 3-connected[34], that is, the removal of any two vertices does not leave the graph disconnected. Hence, by Whitney's unique embedding theorem[35], the generated embedding retains the cyclic order of edges around vertices in the 3D mesh.

The first three modules essentially prepare the mesh for routeing. As detailed in Supplementary Note 1, the desired form of routeing is based on A-trails, where for polyhedral graphs consecutive edges in the circuit always lie on the same face boundary[36]. However, the search for A-trails is expensive, with the problem known to be NP-complete both for general planar graphs[37] and polyhedral graphs[23].

Nevertheless, the last module performs an A-trail search on the embedding based on a systematic branch-and-bound search. The algorithm constructs the search tree based on binary choices for vertices of degree at least six, resulting in an Eulerian circuit in a derived graph with maximum degree four. All the crossings of the circuit that are at degree-four vertices in the derived graph can then be removed in polynomial time[38]. The structuring of the search tree, coupled with a heuristic for branching order, enabled the generation of routeings for large meshes such as those designed in this work. For instance, the routeing for the Stanford bunny, the most complex among the ones designed, was obtained in 87.87 ms (average of 11 runs) on a midrange workstation (Intel Core i5-2500 CPU at 3.30 GHz, 8 GB RAM, Windows 7 64-bit OS). The software code of the modules for the routeing is freely available online at https://github.com/mohamma1/bscor.

In the last step before the import into vHelix, the polyhedral mesh is converted into a DNA design of a discrete size. Here, adequate strand lengths for all edges as well as the position of the helices need to be determined. This is done by iteratively minimizing the overall structural tension, as described below and in more detail in Supplementary Note 2.

To find the optimal translation and orientation of helices along the edges, the placement of these is simulated in a spring–rigid-body setup. By approximating the initially placed DNA helices as rigid-body cylinders and the connectivity between endpoint nucleotides of different helices as spring-joints, the total accumulated separation energy of these can easily be minimized by any rigid-body physics simulation engine. We used the Nvidia PhysX engine (https://developer.nvidia.com/physx-sdk).

In the first iteration, the routed structure is loaded and the length of the rigid edges is discretized as a multiple of base-pair lengths (0.33 nm) given by the mesh size and a user-selected scaling factor. Then the relaxation simulation is run and strain on the connecting springs is calculated.

The relaxation optimization is implemented as an iterative process where the physics simulation, described above, alternates with a length-modification step. In this step, one edge is shortened or lengthened by one base. After this, the simulation is started anew and run until a new minimum is found. If this new minimum is a better fit than the previous one, it replaces the current structure in the search for further modifications. If not, the modification will be discarded and the algorithm will modify another helix to attempt to find a lower accumulated spring energy. After the algorithm has been unable to further successfully optimize the structure, the rotation, translation and length of the helices is extracted from the simulation and joined with the routeing to produce an output file in the format .rpoly. This file can be imported to vHelix for further manipulation and design of the origami structure.

On a midrange workstation, the physical relaxation may take hours to fully complete for some structures. However, it may be interrupted by the user and will then output the latest state for import to vHelix. For the Stanford bunny the relaxation took an average of 20 min 35 s (based on 11 runs) on a midrange workstation (Intel Core i5-2500 CPU at 3.30 GHz, 8 GB RAM, Windows 7 64-bit OS).

vHelix. vHelix is our custom-made plug-in for Autodesk Maya. The plugin allows a user to manipulate a model of DNA in 3D and connect strands together freely. The DNA model is programmed to closely emulate known DNA geometry and Holliday junctions created in vHelix closely recreates crystallography data of DNA[39]. vHelix is used to inspect the final design, and allows the user to make manual edits directly in the 3D model if desired.

When Autodesk Maya is running with the vHelix plug-in, .rpoly files can be directly imported using the import menu in Maya. In the import, the staple-strand breakpoints are positioned. If the import menu is used, vHelix will use its default method and position breakpoints at the middle of each edge creating staple strands that each bind to two half-edges. This is used for the ball structure. To achieve a more sophisticated positioning of the breakpoints the .rpoly file can be imported to vHelix using a MEL command in the Maya script editor:

file -options "nicking_min_length = *x*;nicking_max_length = *y*" -import -type "Text based vhelix" -ra true -mergeNamespacesOnClash false -namespace "*file name*" -pr "*file path*"

where *x*, *y*, *"file name"* and *"file path"* are variables that the user should change to what is applicable for that particular import. The integer *x* controls the minimum-edged length at which breakpoints should be positioned. In meshes with a large spread in edge sizes it is appealing to position the breakpoints on the longer edges. The integer *y* controls the maximum allowed staple-strand length; this limit is normally motivated by the length of oligonucleotides that can be synthesized inexpensively. Often, it is not possible to satisfy both parameters in one structure and the result may be a compromise violating one or both parameters. By using the vHelix feature "export strands" the lengths of the staple strands created can be evaluated. If no sequence is assigned to the structure, the exported file gives a list of question-marked sequences that correspond to the undetermined base sequences of the staple strands together with a name describing the helices connected by the staple strand. The helix names can be found in the outliner of Maya for easy inspection of staple strands. This was used for all structures except the ball. In our experience, the simpler staple-strand design is preferable whenever possible and multi-edge stapling should primarily be used to avoid nicks on very short edges.

If the staple strands generated are not satisfactory, the auto-breakpoint design can be rerun with other parameters or the staple strands can be manually remodelled. Staple strands that are too long can be shortened by the manual introduction of breakpoints by selecting a base at the position of the desired breakpoint and using the feature "disconnect bases". Breakpoints can also be removed by selecting the two adjacent bases and using the feature "connect bases". Using these two features, the breakpoints of the staple strands can be manually remodelled. If no automatic breakpoints are desired the .rpoly file can be imported using large values for *x* and *y*. This will generate staple strands with the maximal possible length as determined by the scaffold routeing with the possibility of manually introducing staple-strand breakpoints. For the rod, nicked torus, helix and stickman, some manual modifications were made to the breakpoints. For the bottle and Stanford bunny, no manual modifications were made.

In vHelix the scaffold and staple strands may appear visually as though they are nicked at junctions although they are actually connected. This may induce stress in the folded structures because the junctions may be more tightened than in the vHelix representation. This can be countered by the feature "auto fill strand gaps" in vHelix. The feature will iterate over the DNA strands to search for gaps between bases. If a gap is found, it will be filled by the addition of extra unpaired bases. This can be performed on a single selected strand or on all staple and scaffold strands if no strand is selected. This was used for all structures except the ball; adenine was used to supply unpaired extra bases. We designed a version of the rod without this feature and found that it did not fold successfully, possibly owing to high tension in the junctions. Therefore we recommend the use of this feature in most designs.

To generate staple-strand sequences the sequence of the scaffold strand is assigned by selecting a base of the scaffold and using the feature "apply sequence". This will automatically assign the complementary sequence to the staple strands. If the used scaffold is longer than needed for the structure, the excess unpaired bases will form a loop at the position selected. This may affect the structural stability and so the position of the loop should be chosen to be where the loop will not interfere with other parts of the structure. After sequences have been assigned, the feature "export strands" can be used to export the sequences of a selected strand or all strands if no selection is made. The sequences are exported in a comma-separated file that can be easily imported to a spreadsheet application. If the feature "auto fill strand gaps" has been used, the extra unpaired bases inserted to the staple strands will appear as question marks in the exported file. They can be converted to a desired nucleotide before staple-strand ordering. For an experienced user, the design process in vHelix can be completed in less than an hour.

Scaffold DNA preparation. *Escherichia coli* strain JM109 was streaked on a lysogeny broth agar plate and grown overnight at 37 °C to produce separate colonies. A single colony was cultured overnight in 25 ml lysogeny broth as a pre-culture. 3 ml of this culture was diluted in 250 ml of 2× Yeast extract Tryptone growth medium (Sigma Aldrich) medium with 5 mM $MgCl_2$ (VWR International) and placed in a shaker at 37 °C. During growth, the optical density at 600 nm was measured repeatedly until it reached 0.5. Then the phage for scaffold was added at a multiplicity of infection of 1, and incubation with shaking continued for an additional 4 h. The culture was transferred to a 250-ml centrifuge bottle and was centrifuged at 4,000*g* for 30 min to pellet the bacteria, and the supernatant containing the phage was centrifuged again at 4,000*g* for 20 min. 10 g of PEG 8000 (Amresco) and 7.5 g of NaCl (VWR International) were added to the supernatant, which was then incubated on ice for 30 min and centrifuged at 10,000*g* for 40 min to pellet the phage. Next, the supernatant was discarded, and the pellet was resuspended in 10 ml of 10 mM Tris (pH 8.5, VWR International) and transferred to a 85-ml centrifuge bottle. 10 ml of a solution with 0.2 M NaOH (VWR International) and 1% SDS (VWR International), was added, mixed gently by inversion and incubated at room temperature for 3 min. Then 7.5 ml of 3 M KOAc (VWR International), pH 5.5, was added, gently mixed by swirling and incubated on ice for 10 min to denature the phage protein coat. The mixture was centrifuged at 16,500*g* for 30 min to pellet the phage protein. The supernatant containing DNA was poured into fresh centrifuge bottles, and 50 ml 99.5% EtOH (Kemetyl) was added, mixed gently by inversion and incubated on ice for 30 min and then centrifuged at 16,500*g* for 30 min to precipitate the DNA. The supernatant was carefully discarded and the pellet was washed with 75% EtOH and air dried at room temperature for 15 min. The pellet was resuspended in 2 ml of 10 mM Tris, pH 8.5, and the concentration and quality were characterized by ultraviolet–visual spectroscopy (NanoDrop, Thermo Scientific) and a 2% agarose gel, respectively.

Staple oligonucleotide preparation. Staple oligonucleotides were purchased from Integrated DNA Technologies. They were delivered desalted in water in 96-well plates at a concentration of 100 μM each. The staple strands were pooled and diluted with water to a working concentration of 400 nM each. Lists of staple-strand sequences are found in Supplementary Tables 2–8.

Folding. In the folding reactions, the scaffold DNA was diluted to 5 nM and the staple strands diluted to 50 nM each, corresponding to a 10× excess of each staple to the scaffold. Scaffold-strand M13mp18 was used for the ball, nicked torus, stickman and bottle, p7560 was used for the helix and bunny, and p8064[15] was used for the rod. For standard folding the mix was brought to 5 mM Tris 1 mM ethylenediaminetetraacetic acid (EDTA, VWR International) and between 4 mM and 10 mM $MgCl_2$. For folding in PBS the sample was mixed with 10× PBS (Sigma Aldrich) to 1× PBS in the final mix. For folding in DMEM the sample was mixed with 10× DMEM (Sigma Aldrich) supplemented with sodium bicarbonate (Sigma Aldrich), as instructed by the manufacturer. The mixed sample was put on a thermal ramp starting with a rapid heat denaturation at 80 °C for 5 min followed by cooling from 80 °C to 60 °C over 20 min, then slow cooling from 60 °C to 24 °C over 14 h.

Agarose gel electrophoresis. Agarose gels were cast using 2% agarose (VWR International) in 0.5× Tris/borate/EDTA (TBE buffer) supplemented with 10 mM $MgCl_2$ and 0.5 mg ml^{-1} ethidium bromide (Sigma Aldrich). Gels were run in 0.5× TBE buffer supplemented with 10 mM $MgCl_2$ on ice at 70 V for 4 h on ice. After running, gels were imaged in a GE LAS 4000 imager.

Gel extraction of structures for electron microscopy. Samples were run in 0.8% agarose gels with 0.5× TBE buffer supplemented with 10 mM $MgCl_2$ and 0.5 mg ml^{-1} ethidium bromide at 90 V until adequate separation was achieved. The band containing well-folded structures was cut out and smashed using a micro-pestle. The smashed band was transferred to a freeze and squeeze gel extraction column (Bio-Rad) and centrifuged at 13,000*g* for 3 min.

Negative-stain transmission electron microscopy. A 400-μl aliquot of 2% w/v uranyl formate (Electron Microscopy Sciences) was mixed with 8 μl of 1 M NaOH and centrifuged at 16,500*g* for 5 min. 3 μl of sample was put on a glow-discharged, carbon-coated, formvar resin grid (Electron Microscopy Sciences) for 20 s before blotting on a filter paper. The sample was spotted in water and blotted again before spotting in the uranyl formate solution for 20 s. After blotting again the sample was air-dried and imaged in a FEI Morgagni 268 at 28,000× magnification.

Cryo-electron tomography. Vitrobot Mk2 (FEI) was used to prepare cryo-specimens for electron microscopy/tomography. 10-nm protein-A-coated gold nanoparticles were applied as fiducial markers for image alignment to Quantifoil R2/2 grids with an additional layer of continuous carbon film after glow-discharge treatment for 20 s. The grids were additionally glow-discharged during the 2 min immediately before application of 3 μl of the sample solution. The grids were incubated at relative humidity of 90% to 100% for one to five minutes and frozen in liquid ethane after blotting (blotting time 2–3 s, drain time 1 s). The grids were transferred into a GATAN 626 cryo-holder and examined in an FEI CM200 FEG microscope under low-dose conditions.

EMMENU software (http://www.tvips.com) was used for automated collection of the tilt series in the range of $-64°$ to $+64°$ with a $4°$ increment. The images were recorded with a TVIPS TemCam F214 charge-coupled device camera at either 6 μm or 9 μm underfocus and a total magnification of 57,000× (pixel size equal to 4.2 Å). The dose used for image acquisition was approximately 2 electrons per $Å^2$ per image. 3D reconstruction was performed using the IMOD package[40]. Two cycles of SIRT refinement (simultaneous iterative reconstructive technique) were applied to increase reconstruction quality.

DNase stability assay. The ball and helix structures were folded in 10 mM $MgCl_2$, 5 mM TRIS, 1 mM EDTA as described. The structures were washed into 1× PBS supplemented with 2.5 mM $MgCl_2$ and 0.1 mM $CaCl_2$ (Sigma Aldrich) three times using a 100 kDA MWCO spin filter (Millipore). DNase I (New England Biolabs) was diluted in the same buffer and added at concentrations of 0.9–57.6 U ml^{-1} (3.6 U ml^{-1} is the average concentration in human blood[41]). The samples were incubated for one or twelve hours at 37 °C and then immediately loaded in a 2% agarose gel supplemented with 10 mM $MgCl_2$ and run for 3 h at 90 V. Gel data (Supplementary Fig. 26) indicates that the structures are stable up to 28.8 U ml^{-1} for one hour and only minor degradation is observed in samples under physiological conditions up to 12 h.

31. Cromwell, P. R. *Polyhedra* 476 (Cambridge Univ. Press, 1999).
32. Jungnickel, D. *Graphs, Networks and Algorithms* Vol. 8, 695 (Springer, 2012).
33. Boyer, J. M. & Myrvold, W. J. On the cutting edge: simplified *O*(*n*) planarity by edge addition. *J. Graph Algorithms Appl.* **8,** 241–273 (2004).
34. Ziegler, G. M. *Lectures on Polytopes* 370 (Springer, 1995).
35. Fleischner, J. & Fleischner, H. *Eulerian Graphs and Related Topics* Part 1, Vol. 1, 407 (Elsevier, 1990).
36. Andersen, L. D., Fleischner, H. & Regner, S. Algorithms and outerplanar conditions for A-trails in plane Eulerian graphs. *Discrete Appl. Math.* **85,** 99–112 (1998).
37. Bent, S. W. & Manber, U. On non-intersecting Eulerian circuits. *Discrete Appl. Math.* **18,** 87–94 (1987).
38. Tsai, M.-T. & West, D. B. A new proof of 3-colorability of Eulerian triangulations. *Ars Math. Contemp.* **4,** 1 (2011).
39. Ortiz-Lombardia, M. *et al.* Crystal structure of a DNA Holliday junction. *Nature Struct. Biol.* **6,** 913–917 (1999).
40. Kremer, J. R., Mastronarde, D. N. & McIntosh, J. R. Computer visualization of three-dimensional image data using IMOD. *J. Struct. Biol.* **116,** 71–76 (1996).
41. Cherepanova, A. *et al.* Immunochemical assay for deoxyribonuclease activity in body fluids. *J. Immunol. Methods* **325,** 96–103 (2007).

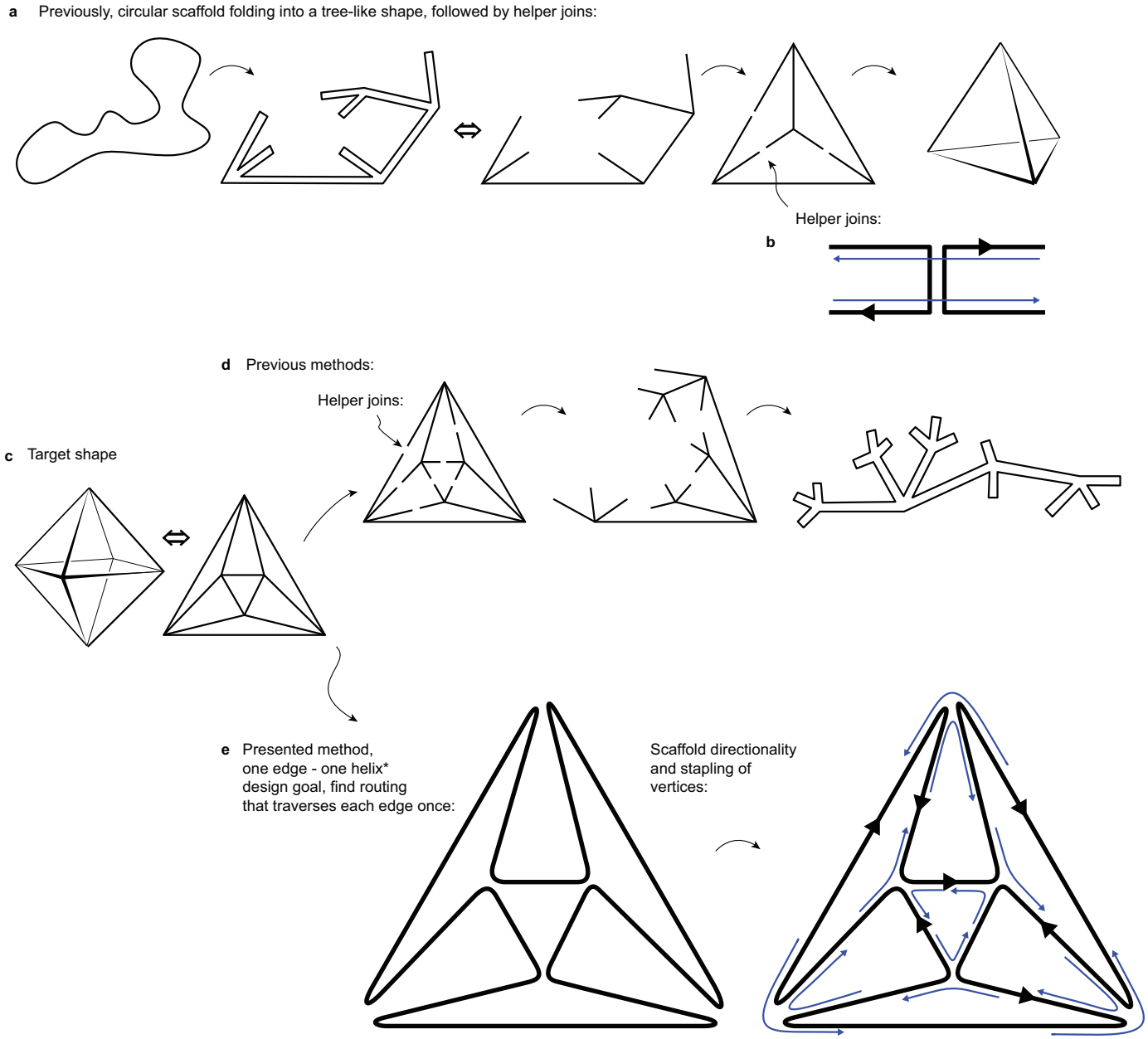

Extended Data Figure 1 | Comparison with previous strategy for polygonal DNA origami. a, Previous strategies for folding polygonal DNA origami have relied on folding the circular single-stranded DNA into a tree-like shape, where each branch is composed of an even number of helices (two in this illustration), these branches are then connected using helper joins as in **b**, where staple strands (in blue) bridge the gap between the distant parts of the scaffold, to yield the final polyhedral structure: the tetrahedron to the right in this example. **c**, The target shape and its flattened Schlegel representation. **d**, Previous methods have introduced helper joins in $N - 1$ of the edges, where N is the number of faces in the structure. Notably, the structures presented in this work would require on the order of 100 helper joins. A large number of helper joins is commonly believed to increase aggregation problems owing to the sticky ends produced as intermediates during folding. **e**, The strategy presented in this work. The goal is to route the entire scaffold through all the edges of the mesh, without crossing and with preferably only one traverse per edge. *It turns out that one helix per edge is not possible for all meshes (as described in the main text, Fig. 1 and in Supplementary Note 1). Odd-degree vertices require some edges to be traversed twice by the scaffold routeing.

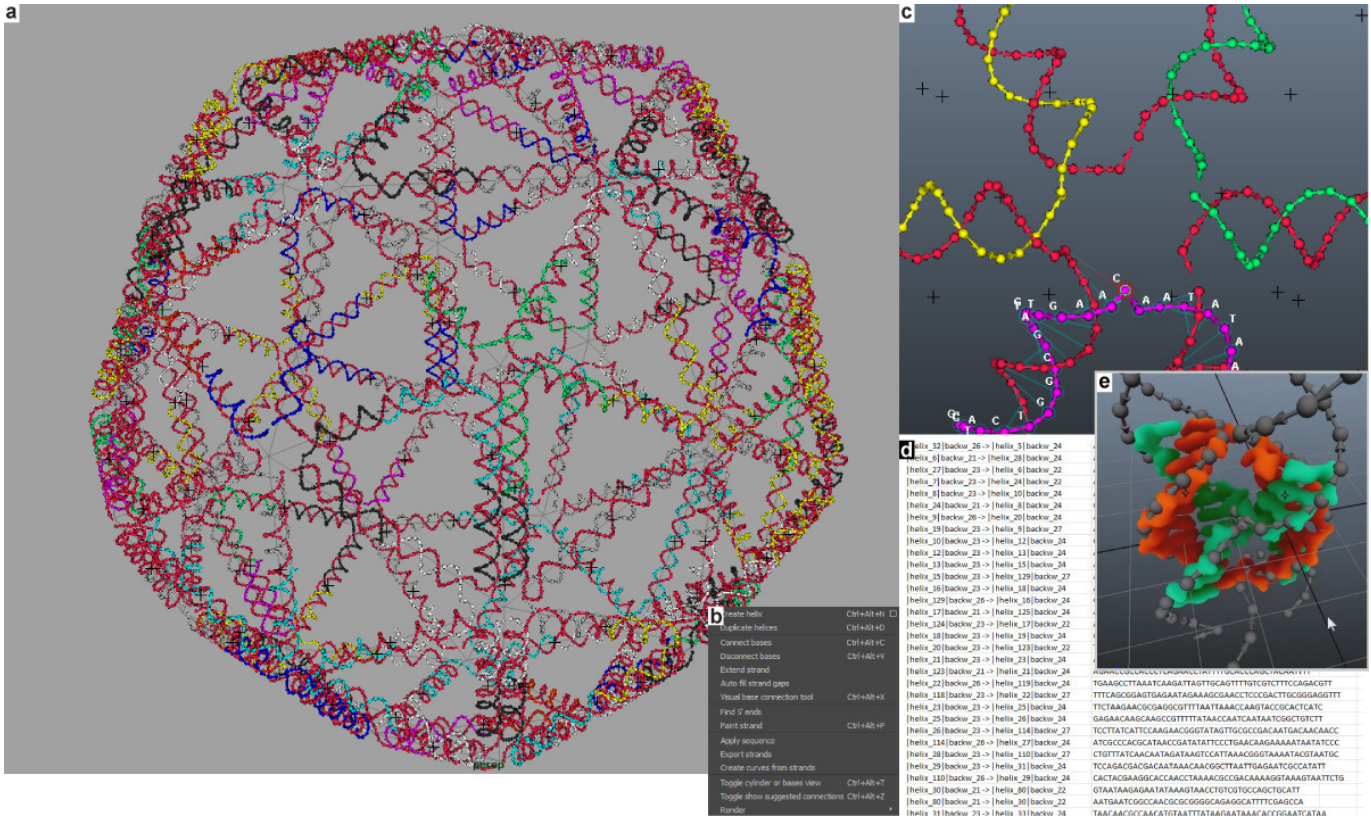

Extended Data Figure 2 | An overview of vHelix. To be able to work with non-canonical origami designs, we implemented software that would allow free-form manipulation of helices directly in 3D space. The software was implemented as a plug-in for Autodesk Maya (several versions) and is available at http://www.vhelix.net. The associated source code can be found at https://github.com/gardell/vHelix. **a**, The interface in vHelix when viewing the design of the ball structure. **b** The 'Helix' menu provides most of the functionality, such as the ability to create new helices, disconnect and connect bases. **c**, Close-up of a connected vertex. Selecting a base shows its associated connectivity by highlighting all connected bases and displaying the associated sequence if a sequence has been applied. **d**, Using the "apply sequence" command to one of the strands (the scaffold), the plug-in calculates the sequence of all paired bases (on the staple strands) and subsequently the command "export strands" generates a spreadsheet file containing the staple-strand sequences. The physical dimensions of the DNA model follows what is usually used in DNA nanotechnology design processes (that is, a 2-nm helical radius, a 0.334-nm rise, a 34.286° pitch and a 155° minor groove). **e**, Overlaying the model with crystallography data from the literature[39] shows that the model fits natural DNA well.

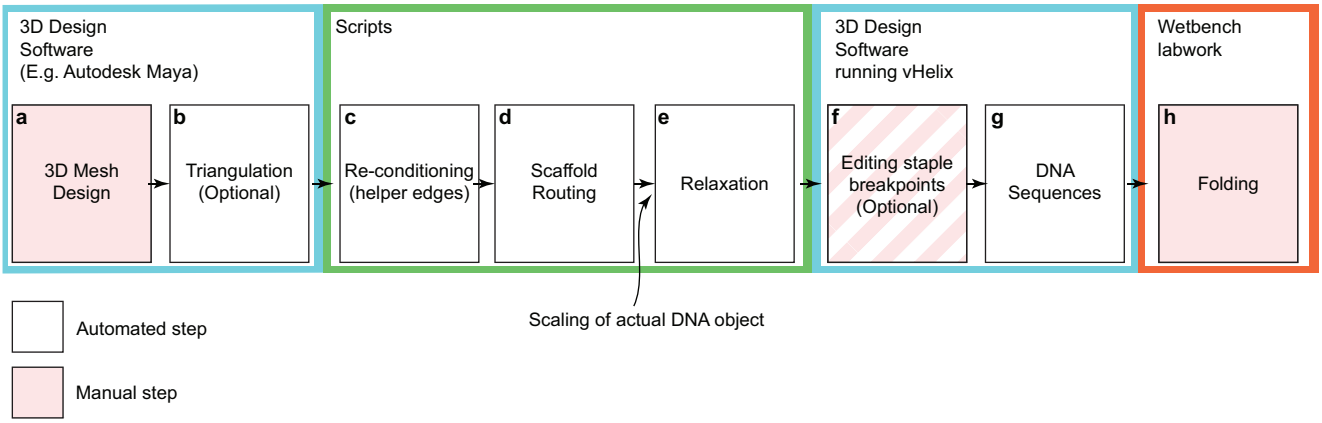

Extended Data Figure 3 | Design pipeline overview. a, We started the designs in Autodesk Maya, importing or modelling our own 3D polygon mesh object. **b**, The triangulation step is not mandatory because the scaffold routeing and further processing is not limited to triangulated meshes, but it is used for all structures reported here to achieve extra rigidity by triangulation. Steps **c**–**e** are implemented as a series of scripts that process the mesh exported from the 3D design software. **c**, All odd-degree vertices are joined by helper edges using a minimum weight perfect matching algorithm (see Supplementary Note 1). **d**, The re-conditioned mesh is fed to a script implementing the A-trails routeing algorithm (see Supplementary Note 1). **e**, After scaffold routeing, the physical relaxation model reads the routed path. Up until now, the mesh has been treated as an abstract graph; in the relaxation step, however, an input is required to set the physical size of the desired DNA rendering, that is, the user sets a scaling value to fit the mesh to the scaffold available for the folding. The relaxation simulation and length-modification scheme (described in more detail in Supplementary Note 2) will rotate and shorten/lengthen some edges to find an overall best fit to the desired 3D shape while accounting for strain between nucleotides in the vertices. The output of the relaxation/length modification optimization is a file readable by vHelix, a plug-in for Autodesk Maya. **f**, As the file is imported into vHelix, the user has the option of automatically positioning staple-strand break-points by stating parameters for maximum staple length and the minimum length of edges with breakpoints. Alternatively, the staple-strand breakpoints can be edited manually in vHelix after importing. **g**, The DNA sequences of all staple strands given a scaffold input is calculated and exported to a spreadsheet by vHelix. **h**, The mixing of staple strands and scaffold is done by hand but a pipetting robot could conceivably also make this last step highly automated.